Article

Effect of the Geometrical Structure on the Superhydrophobicity and Self-Cleaning Properties of Plasma-Treated Polyvinylidene Fluoride Fabrics

Hyae Rim Hong, Joon Seok Lee, and Chung Hee Park*

Read Online

ACCESS | Metrics & More | Article Recommendations | SI Supporting Information

ABSTRACT: The purpose of this study is to develop super-hydrophobic polyvinylidene fluoride (PVDF) fabrics to increase their water repellency and self-cleaning properties and to investigate the effects of the inherent fabric roughness on these properties. A PVDF fabric, composed entirely of electrospun PVDF filament yarns, and two PVDF/polyester (PET) fabrics with different weave densities are used. After treatment with O_2 plasma for 12 min and CF_4 plasma for 4 min, superhydrophobicity is achieved in all fabrics, resulting in an increase in water repellency and self-cleaning efficiency. The PVDF fabric with the lowest shedding angle exhibits the most pronounced droplet rebound behavior and the highest self-cleaning efficiency. Increases in surface inclination angle and droplet volume and a decrease in the drop fall height all contribute to conditions more favorable for water droplet repellency. The self-cleaning efficiencies of the plasma-treated PVDF fabric and high-density PVDF/PET fabric are higher for hydrophilic dust, in contrast to those of the untreated ones. The findings of this study are expected to enable the design of weaving or nano-structuring conditions that enhance the water repellency and self-cleaning properties of PVDF fabrics, for the development of stable energy-harvesting smart textiles.
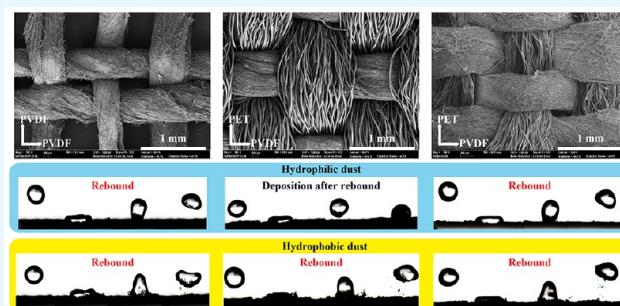
1. INTRODUCTION

A water droplet placed on a superhydrophobic surface easily rolls down the surface at a relatively shallow angle of less than 10°; the contact angle is greater than 150°.[1] Numerous fabrication methods have been explored to achieve super-hydrophobicity, such as photolithography, etching, and nano-particle deposition for roughening the surface and vapor deposition, spraying, dip-coating, and grafting with chemicals for lowering the surface free energy.[2,3] Superhydrophobicity endows surfaces with self-cleaning abilities, wherein droplets adsorb any contaminants present on the superhydrophobic surface and then roll along the surface, removing the contaminants.[4] A superhydrophobic surface with a high water repellency can also prevent liquid wetting, condensation, ice formation, and corrosion[5−7] and therefore finds applications in a variety of fields, including electronic devices and materials for smart clothing.

In recent years, superhydrophobic modification has been widely employed in energy harvesters that rely on contact electrification at the liquid−solid interface (i.e., triboelectric nanogenerators [TENGs]).[8,9] When a water droplet comes in contact with a surface and then detaches, triboelectric charges are generated on the surface and electricity can be harvested via the electrostatic induction caused by these surface charges.[9] In this context, Cho et al.[9] investigated the dependence of the

output performances of liquid−solid contact TENGs on the dynamic behaviors of droplets on superhydrophobic aluminum surfaces with hierarchical rough structures. They found that droplets were retained on surfaces with nanoscale roughness, and the output performances of the TENGs decreased as the number of falling droplets increased. Meanwhile, the droplets were completely detached from surfaces with micrometer (μm) and nanometer (nm) roughness, thereby significantly enhancing the output performance. Due to the fact that the output performance of a TENG is generally reduced when the surface is exposed to moisture or pollutants,[10−13] it is necessary to endow the surface with water-repellent and self-cleaning properties to overcome this limitation.

Polyvinylidene fluoride (PVDF) is frequently employed as the material for use in TENGs owing to its high electron affinity, high flexibility, and excellent biocompatibility, which result in highly negative triboelectric properties and render this material suitable for use in smart clothing.[14] However, to date, PVDF has
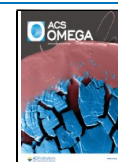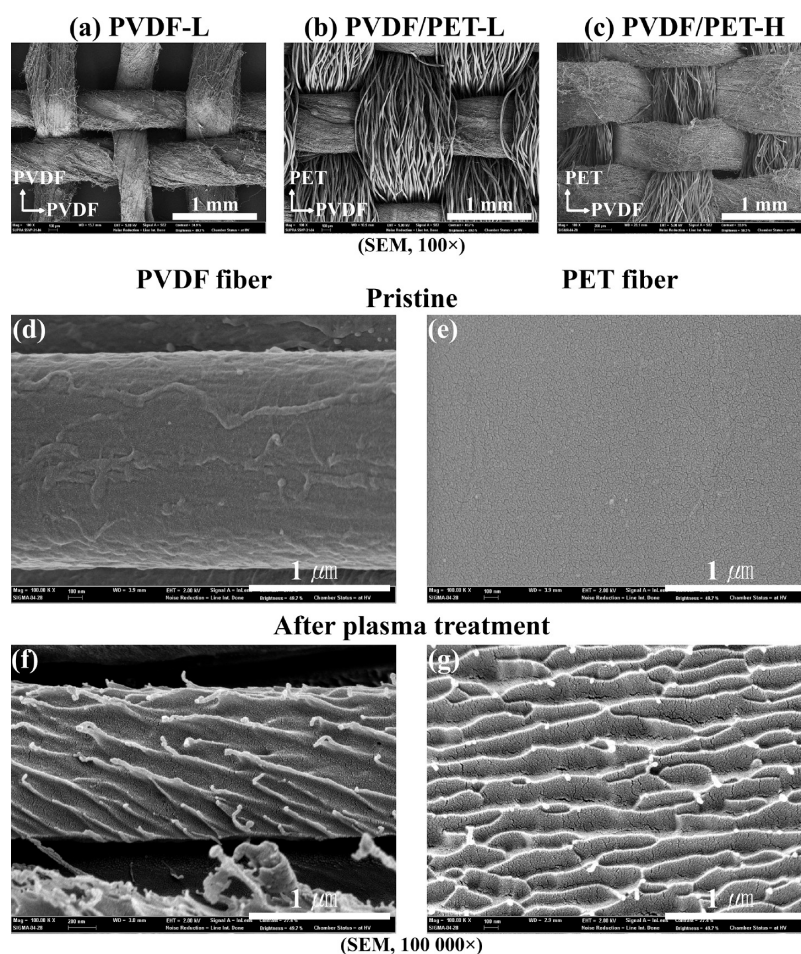
Figure 1. Surface morphologies of the PVDF specimens. (a−c) Pristine surfaces of the PVDF fabrics, and (d−g) nanoscale roughness introduced after plasma treatment on the surface of PVDF fiber and PET fiber in PVDF/PET-H. Field emission (FE)-SEM images are shown at magnifications of 100× for each fabric and 100 000× for each fiber.

primarily been used in the form of films or electrospun nanowebs, and only a few studies have investigated its application as a woven fabric.[15−18] It is expected that the weaving conditions of such a fabric will affect its inherent microstructure and lead to variations in the superhydrophobicity, which in turn will affect the dynamic behavior of droplets on the surface and the self-cleaning properties of the fabric. However, previous studies have primarily focused on uniform, non-porous substrates, such as films, and the water repellency of these substrates was typically evaluated in terms of dynamic contact angles, such as the shedding angle or the sliding angle.[2,19] It is, therefore, necessary to analyze the dynamic behaviors of droplets on the surfaces of superhydrophobic fabrics in a variety of environments to determine the most favorable fabric structure and environment for complete droplet repellency.

Thus, to develop wearable energy harvesting PVDF textiles resistant to moisture and pollutants, we intended to enhance the water repellency and self-cleaning properties of fabric through superhydrophobic modification. For this purpose, a 100% PVDF fabric and two PVDF/polyester (PET) fabrics with different weave densities are used to investigate the effect of the inherent fabric structure under various weaving conditions. Plasma treatment is the most commonly used method for enhancing the output performance of TENGs;[20−22] it is a simple and human-friendly process that can increase the roughness of fiber

without a mask and does not require further chemical treatment.[23,24] Therefore, plasma treatment is employed to impart superhydrophobicity considering the application of PVDF fabrics. The fabrics are subsequently treated with O_2 plasma for 12 min and CF_4 plasma for 4 min, and the contact and shedding angles are measured to ensure that superhydrophobic surfaces are achieved. In addition, the dynamic behaviors of the droplets are examined on the fabric surfaces by varying the drop fall height, the surface inclination angle, and the droplet volume. Furthermore, the self-cleaning properties of the fabrics are estimated using iron oxide and Sudan black B particles as hydrophilic and hydrophobic dusts, respectively. Ultimately, our aim is to develop effective weaving and treatment methods to enhance the water repellency and self-cleaning properties of PVDF fabrics.

2. RESULTS AND DISCUSSION

2.1. Surface Structures and Chemical Compositions.
The pristine surface of each fabric was observed at a magnification of 100× using scanning electron microscopy (SEM), and the obtained images are shown in Figure 1a−c. The PVDF filament yarn used in all fabrics was composed of a one-way electrospun fiber with a thickness of ~1 μm, and the total thickness of each PVDF yarn was 524−598 μm. The average thicknesses of the PET filament yarns in the PVDF/PET fabric with low density (PVDF/PET-L) and high density (PVDF/

PET-H) were 807 and 665 μm, respectively, and the yarns were constructed using PET fibers with average thicknesses of 22 and 12 μm. The mean deviations of the surface geometrical roughness values and the area percentages of the direct open pores in the images are summarized in Table 1. It was found that PVDF-L contained the highest area percentage of direct open pores, whereas PVDF/PET-H contained the lowest (Figure S1, Supporting Information).

Table 1. Geometrical Roughness of the Pristine Specimens

	SMD [μm][a]	area percentage of direct open pores [%]
PVDF-L	3.20 ± 1.65	16.5 ± 5.8
PVDF/PET-L	2.78 ± 1.62	10.4 ± 1.7
PVDF/PET-H	3.56 ± 1.06	4.6 ± 0.1

[a]SMD: surface mean deviation, a measure of the geometrical roughness.

High-magnification SEM images (×100 000) revealed the fine structures of the fibers after O_2 and CF_4 plasma treatment. As shown in Figure 1d−g, nanoscale roughness was developed on the surfaces of the PVDF and PET fibers with a spacing of approximately 230−287 nm. Additionally, energy dispersive X-ray spectroscopy (EDS) and X-ray photoelectron spectroscopy (XPS) analyses showed high fluorine content on the PVDF and PET fibers, and the emergence of new peaks such as −CHF, CF_2−CHF, and CF_3−CHx (Figures 2 and S3, and Table S1).[25,26] Furthermore, the peak corresponding to fluorine in the XPS broadened and shifted by +0.5 eV,[27] confirming that the PVDF and PET surfaces were successfully fluorinated by CF_4 plasma treatment. As indicated above, the observed nanoscale roughness and fluorinated surfaces are both favorable for achieving superhydrophobic materials.

The surface wettability of each fabric before and after plasma treatment was also measured, and the results are presented in Table 2. Specifically, prior to plasma treatment, the PVDF-L and PVDF/PET-H possessed greater static contact angles than PVDF/PET-L, and the shedding angle increased in the order of PVDF-L < PVDF/PET-H < PVDF/PET-L. This was accounted for by considering that PVDF and PET possessed hydrophobic and rough surfaces, and therefore, the greater the number of air layers in contact with the water droplets, the larger the static contact angle.[28−30] In addition, PVDF-L, which was composed entirely of PVDF, exhibited lower surface energy and the highest area percentage of direct open pores, while PVDF/PET-H possessed the highest surface roughness (Table 1). Thus, PVDF-L and PVDF/PET-H exhibited greater static contact angles, and the lower adhesive energy was attributed to the smaller contact area of the water droplet on the surface.[31]

As indicated in Table 2, following plasma treatment, the static contact angle increased to ≥150° in all cases, while the shedding angle decreased significantly to ≤10°, thereby suggesting that superhydrophobicity was achieved for all fabrics. This was attributed to the introduction of nanoscale roughness during plasma treatment, which minimized the contact areas between the droplets and the sample surfaces.[23,24] In addition, the surface energy of the surface roughened by O_2 plasma treatment was further decreased by fluorination during the subsequent CF_4 plasma treatment (Figures S2−S4 and Table S1). Furthermore, the shedding angles for the various fabrics before and after plasma treatment followed the same order, that is, PVDF-L < PVDF/PET-H < PVDF/PET-L, thereby indicating that the observed superhydrophobicity was a result of dual-scale surface

roughness on both the micro- and nanoscales. In the case of the PVDF film, after the same plasma treatment, the water drop adhered to the surface even when the contact angle increased over 150° (Figure S5), demonstrating the significance of the microscale roughness of fabric. It should be noted here that the inherent microscale roughness of the surface is advantageous to achieving superhydrophobicity, and it also appears to affect the surface wettability even after plasma treatment.

The effect of plasma treatment on the mechanical properties of the developed superhydrophobic fabric was also evaluated for PVDF/PET-H (Tables S2 and S3 and Figures S6−S8). Although the plasma treatment caused decreases in tensile strength and elongation at break, it did not significantly affect the stiffness and color, and air and water vapor permeabilities were maintained at a high level (Table S3). In addition, the contact angle remained more than 160° after laundering, tape test, and abrasion with nylon knit. Furthermore, even after repeating the abrasion with nylon knit 30 times, PVDF/PET-H demonstrated superhydrophobicity as the shedding angle was low (6.2 ± 0.8°). These results indicate that the plasma-treated superhydrophobic fabric provides wearing comfort with excellent flexibility and breathability, and stable superhydrophobicity against abrasion; thus, it is a promising material for smart textiles.

2.2. Dynamic Behaviors of the Water Droplets on the Fabric Surfaces.

Zimmermann et al.[19] developed a method to measure the shedding angles of superhydrophobic textiles to evaluate their water-repellent properties. However, even when a surface is determined to be superhydrophobic based on the shedding angle, it has been shown that the water repellency of the fabric can vary significantly depending on the external conditions under which the water droplet is applied.[32,33] Thus, considering that the superhydrophobic textile is used for clothing materials to be worn in various environments, we investigated the effects of the drop fall height, the surface inclination angle, and the droplet volume to examine the dynamic behaviors of the droplets on the PVDF-L, PVDF/PET-L, and PVDF/PET-H specimens, as depicted in Figure 3, where the x-axis represents the surface inclination angle and the y-axis represents the droplet volume.

For all fabrics, a more complete rebound was observed when the fall height was reduced from 15 to 1 cm, or when the surface inclination angle was increased from 15 to 60°. Additionally, a greater degree of rebound occurred with larger droplet volumes, and the largest droplet tended to exhibit a partial rebound. Compared to the pristine specimens, more complete rebound (denoted as cR (yellow) in Figure 3) was observed after plasma treatment, and the degree of rebound decreased in the following order: PVDF-L > PVDF/PET-H > PVDF/PET-L. Importantly, when the surface of PVDF-L was tilted by ≥30° and the drop fall height was 15 cm, complete rebound of the droplets was observed on the plasma-treated surfaces.

The dynamic behavior of a droplet on a surface is determined by the relationship between the wetting pressure required to moisten the surface and the anti-wetting pressure required to repel the droplet.[34] In terms of the wetting pressure, the effective water hammer pressure (P_{WH}) when the water droplet impinges on the surface and the dynamic pressure (P_D) at the spreading stage of impingement were considered. These pressures can be represented as shown in eqs 1 and 2, respectively[35]
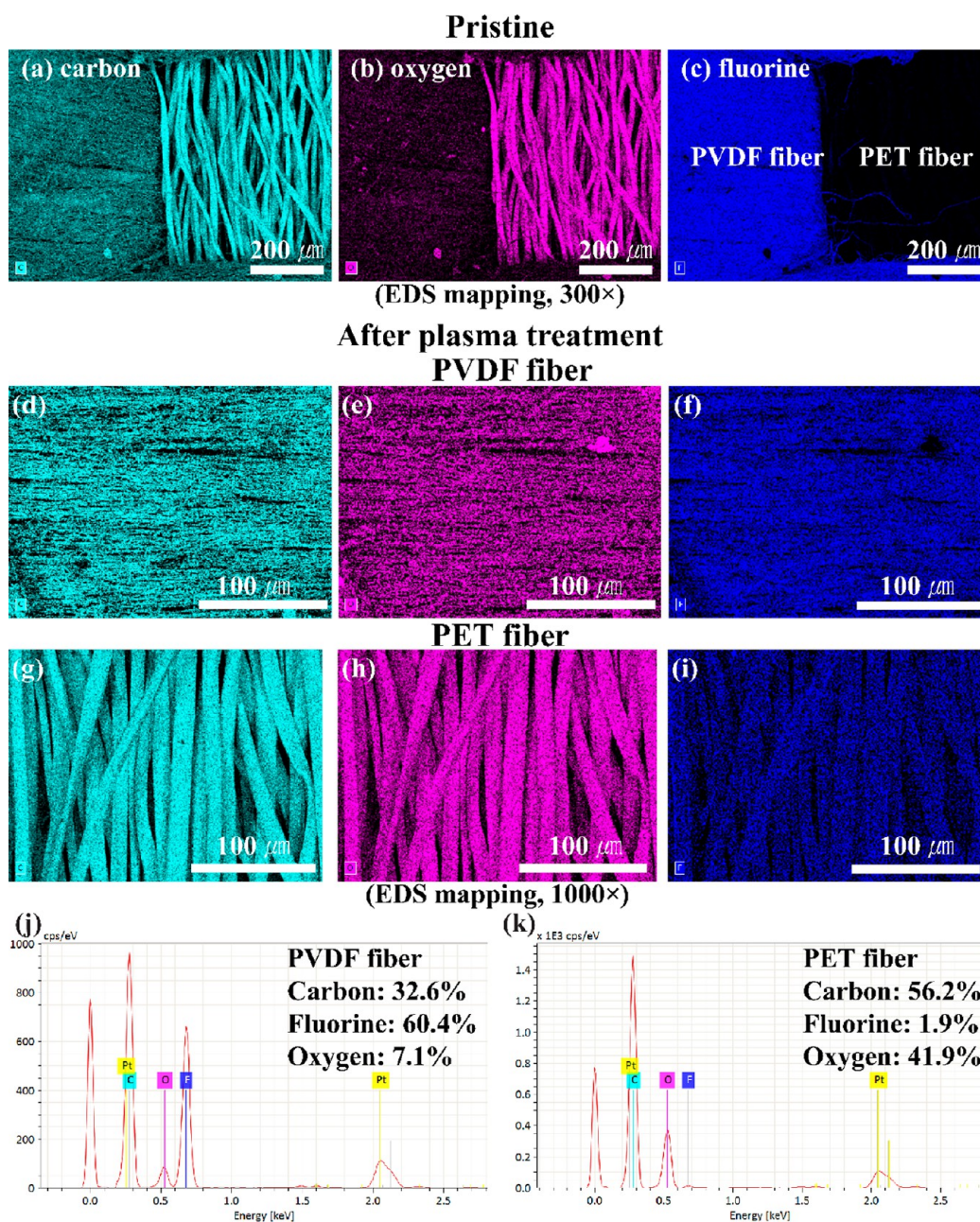
$$P_{WH} \approx 0.2\rho CV \tag{1}$$

Figure 2. Changes in the surface chemical compositions of the PVDF specimens. (a−c) Pristine PVDF/PET-H, (d−f) PVDF fibers, and (g−i) PET fibers after plasma treatment. Mass normalized concentrations (%) of the atoms constituting (j) PVDF fiber and (k) PET fiber quantitatively analyzed based on the EDS profiles at magnifications of 1000×.

Table 2. Surface Wettability Properties of the Specimens before and after Plasma Treatment

	contact angle [°]		shedding angle [°]	
	pristine	after plasma	pristine	after plasma
PVDF-L	151.8 ± 2.7	160.0 ± 3.2	31.1 ± 3.8	3.3 ± 1.2
PVDF/PET-L	142.7 ± 3.8	159.2 ± 4.1	41.3 ± 4.0	10.5 ± 1.8
PVDF/PET-H	152.2 ± 3.4	163.7 ± 1.2	32.4 ± 4.3	4.6 ± 0.7

$$P_D = \frac{1}{2}\rho V^2 \tag{2}$$

where ρ is the density of the droplet, C is the velocity of sound in water ($C \approx 1497$ m/s), and V is the impinging velocity of the droplet. Overall, the wetting pressure is proportional to the impinging velocity. In addition, the anti-wetting pressure is considered to be the capillary pressure (P_C) generated between the roughness structure on the surface and can be represented as outlined in eq 3[35]

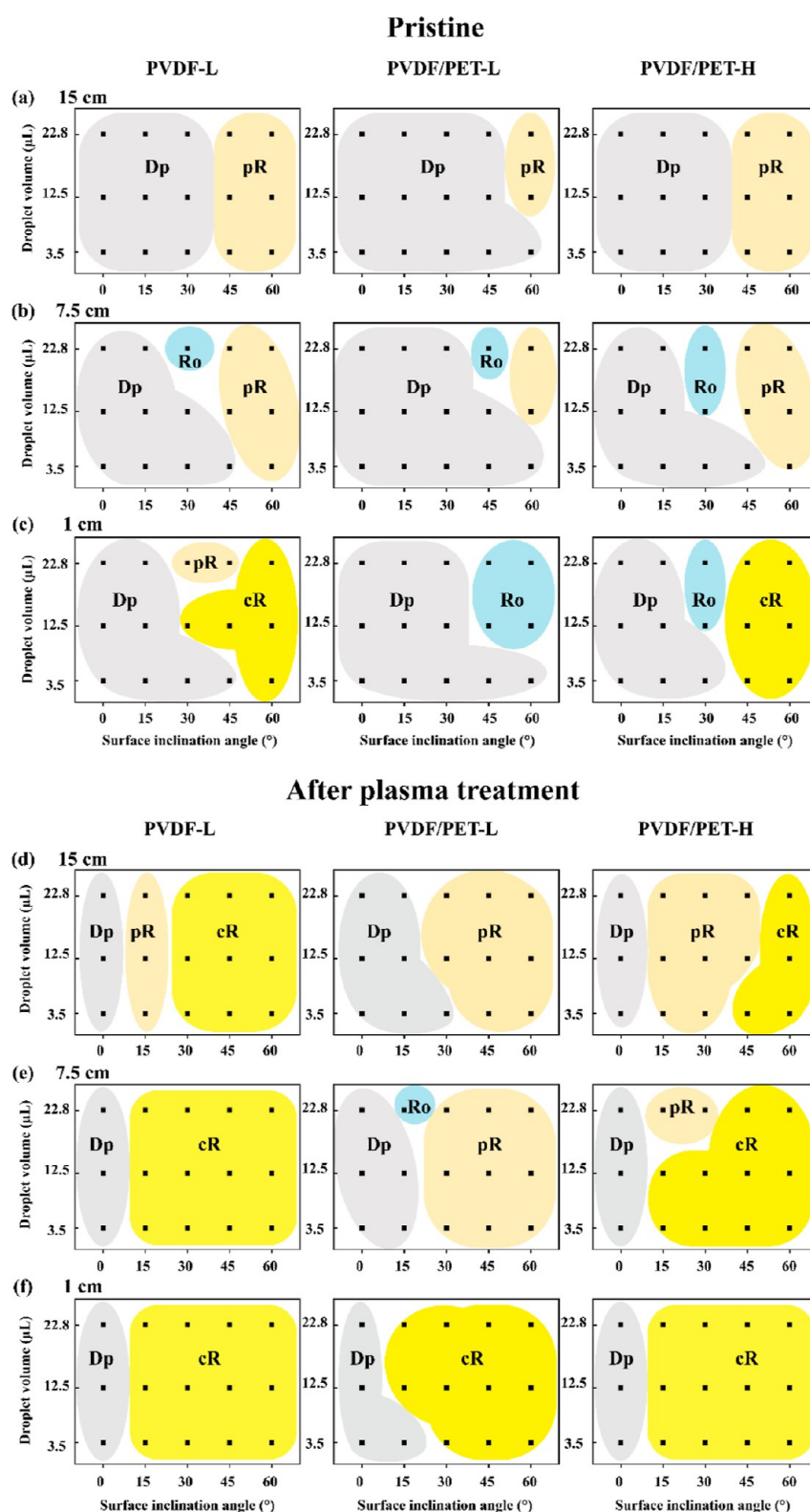$$P_C = -2\sqrt{2}\,\gamma_{LA}\cos\theta_A/S \tag{3}$$

Figure 3. Effects of superhydrophobicity on the droplet impact dynamics on the surfaces of the prepared PVDF specimens. The dynamic behaviors of droplets falling from heights of (a,d) 15 cm, (b,e) 7.5 cm, and (c,f) 1 cm were categorized into deposition (Dp), roll (Ro), partial rebound (pR), and complete rebound (cR) by varying the surface inclination angle (0, 15, 30, 45, or 60°) and the droplet volume (3.5, 12.5, or 22.8 μL) on the surface (a–c) before and (d–f) after plasma treatment.

where γ_{LA} is the surface tension of the water droplet, S is the distance between surface roughness elements, and θ_A is the advancing contact angle of the water droplet on the flat surface, which was determined by measuring the contact angle with

PVDF film (Figure S5). Overall, the capillary pressure is inversely proportional to the distance between the surface roughness elements. Given that the anti-wetting pressure must be greater than the wetting pressure for the surface to completely
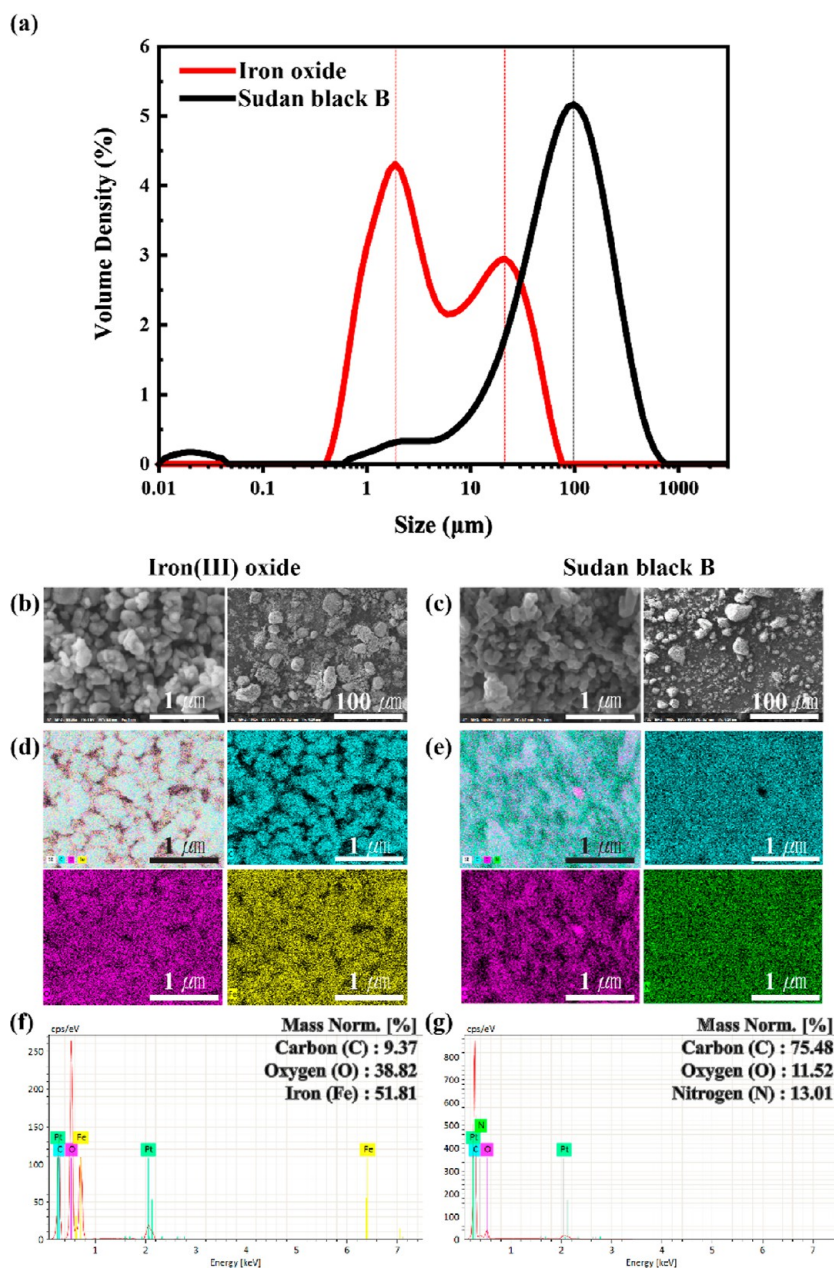
Figure 4. Characteristics of (b,d,f) the iron(III) oxide particles and (c,e,g) the Sudan black B particles. (a) Size distributions based on the volume density analyzed using a laser diffraction particle size analyzer. (b,c) Surface morphologies and (d−g) chemical compositions. FE-SEMimages at magnifications of 1000× and 100 000× with corresponding EDS mapping results and profiles. *C: carbon (sky blue), O: oxygen (pink), Fe: iron (yellow), and N: nitrogen (green).

repel water droplets, a slow impinging water droplet velocity and a small distance between the surface roughness elements are associated with a superior droplet repellency. As a result, the generation of nanoscale structures and the reduced distance between surface roughness that were imparted by the plasma treatment, therefore, enhanced the water repellencies of the fabrics. In this context, Chen et al.[34] calculated the theoretical pressure using the above equations when water droplets were dropped at a velocity of 0.51 m·s^{-1} onto a superhydrophobic surface with dual-scale roughness. Based on their calculation, the P_{WH} was greater than the P_C generated by the microscale roughness (P_{CM}) but smaller than the P_C generated by the nanoscale roughness (P_{CN}). Accordingly, when a droplet contacts the surface, it can penetrate the microscale roughness

on the fabric but cannot penetrate the nanostructured roughness, thereby indicating that plasma treatment can effectively enhance the capillary pressure to facilitate a complete rebound.

As outlined in Table 1, PVDF-L possesses the highest percentage of direct open pores of the various specimens prepared herein, which suggests that it has the smallest contact area for water droplet contact. Indeed, this agrees well with the observation that complete rebound occurs most frequently on PVDF-L. Comparatively, PVDF/PET-H demonstrates more complete rebound than PVDF/PET-L owing to its prominent surface roughness. It is believed that when a water droplet strikes the PVDF/PET-H surface, it initially impinges on the protruding parts of the rough surface, resulting in pressure
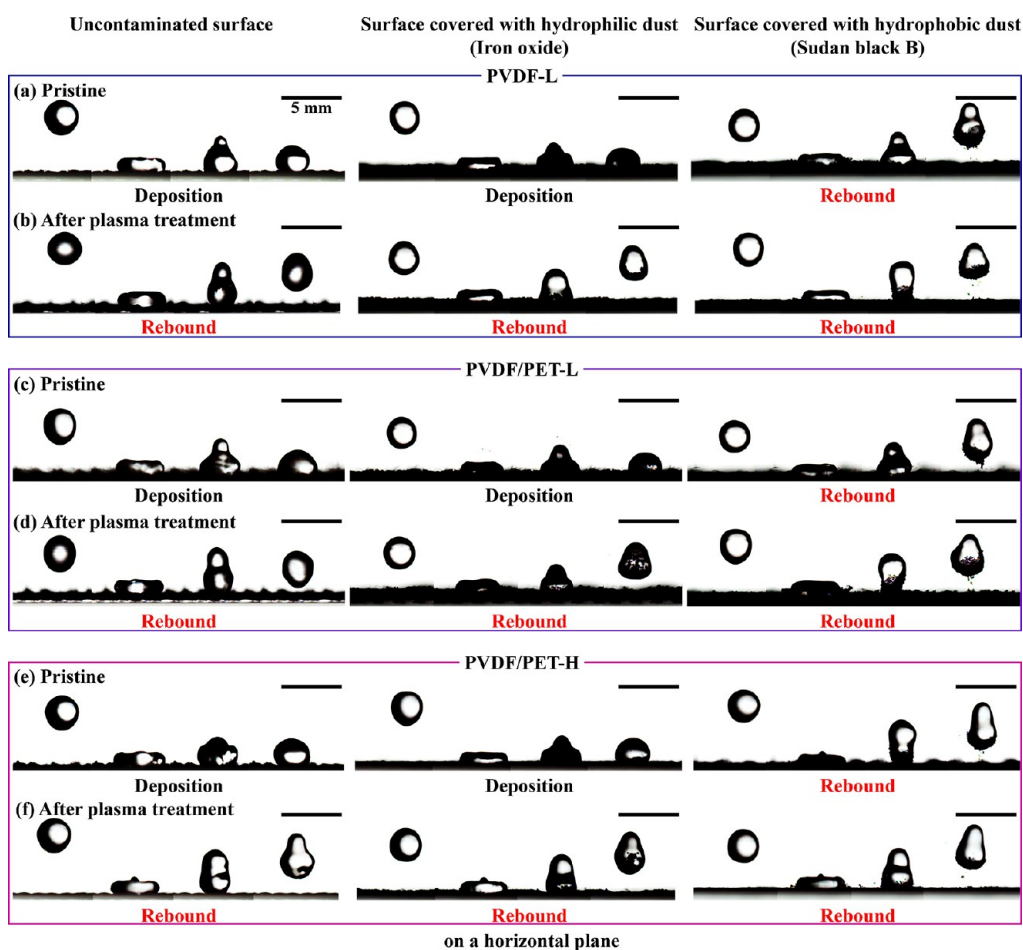
Figure 5. Effects of hydrophilic dust (iron oxide) and hydrophobic dust (Sudan black B) on the dynamic behaviors of droplets on the surfaces of (a,b) PVDF-L, (c,d) PVDF/PET-L, and (e,f) PVDF/PET-H, (a,c,e) before and (b,d,f) after plasma treatment, when a water droplet (12.5 μL volume) fell on a horizontal plane from a height of 1 cm. The scale bar in each image represents 5 mm. The surface inclination angle was 0°.

loss. As a result, the droplets have insufficient energy to penetrate the fabric surface.[34]

It should also be noted that a lower drop fall height and greater surface inclination angle (i.e., α, 15 $\leq$ α $\leq$ 60°) result in a more complete rebound. This can be attributed to the fact that the velocity of the droplet impinging on the surface is reduced proportionally to cos α,[36] resulting in a lower wetting pressure. In addition, the probability of deposition was the highest for the smallest droplets with a volume of 3.5 μL. These droplets have a diameter of 1.9 mm, which is similar to the length of the repeating unit of warp and weft interlaying for the various fabric specimens (Figure 1a−c). However, when the droplet volume was increased to 22.8 μL, the possibility of partial rebound increased. This was due to the larger droplets being more easily deformed, ultimately resulting in droplet trapping between the pores or yarns, wherein some droplets also remain on the surface when the wetting pressure is relatively high.

2.3. Self-Cleaning of Dust Particles on the Fabric Surfaces by the Action of Water Droplets. Iron oxide and Sudan black B were used as dust particles to investigate the self-cleaning properties of the fabrics. The size distribution, surface morphology, and composition of each type of particle are represented in Figure 4. As shown in Figure 4a, the particle size of iron oxide ranged between 0.460 and 66.9 μm, wherein a bimodal distribution with peaks at ∼1.9 μm and 21.2 μm was apparent. The particle size of Sudan black B ranged from 0.0114

to 666 μm, and in this case, a unimodal distribution with a peak at ∼98.1 μm was observed. According to EDS analysis of the particle surface compositions (Figure 4d−g), oxygen and iron accounted for ∼91% of the surface in the case of iron oxide, whereas carbon accounted for ∼75% of the surface of Sudan black B. Thus, iron oxide was considered to be hydrophilic, whereas Sudan black B was considered to be hydrophobic.

The effects of the hydrophilic or hydrophobic dust on the dynamic behaviors of droplets on each fabric surface were then investigated by dropping a 12.5 μL droplet from a height of 1 cm. The corresponding images are presented in Figures 5 and 6, with surface inclination angles of 0 and 15°, respectively. For all pristine fabrics, contamination with the hydrophilic dust led to the same pattern observed before contamination (i.e., deposition), regardless of the surface inclination angle. In contrast, when the surfaces were contaminated with the hydrophobic dust, the water droplets rebounded in all fabrics both before and after plasma treatment.

In the case of the plasma-treated PVDF/PET-L with an inclination angle of 15°, the water droplets were found to rebound before contamination, while after deposition of the hydrophilic dust, they exhibited rebound followed by deposition (Figure 6d). Indeed, it was relatively difficult to separate the droplet from the PVDF/PET-L surface, possibly due to its high shedding angle (Table 2) and the presence of the hydrophilic dust; these factors ultimately reduced the kinetic energy of the
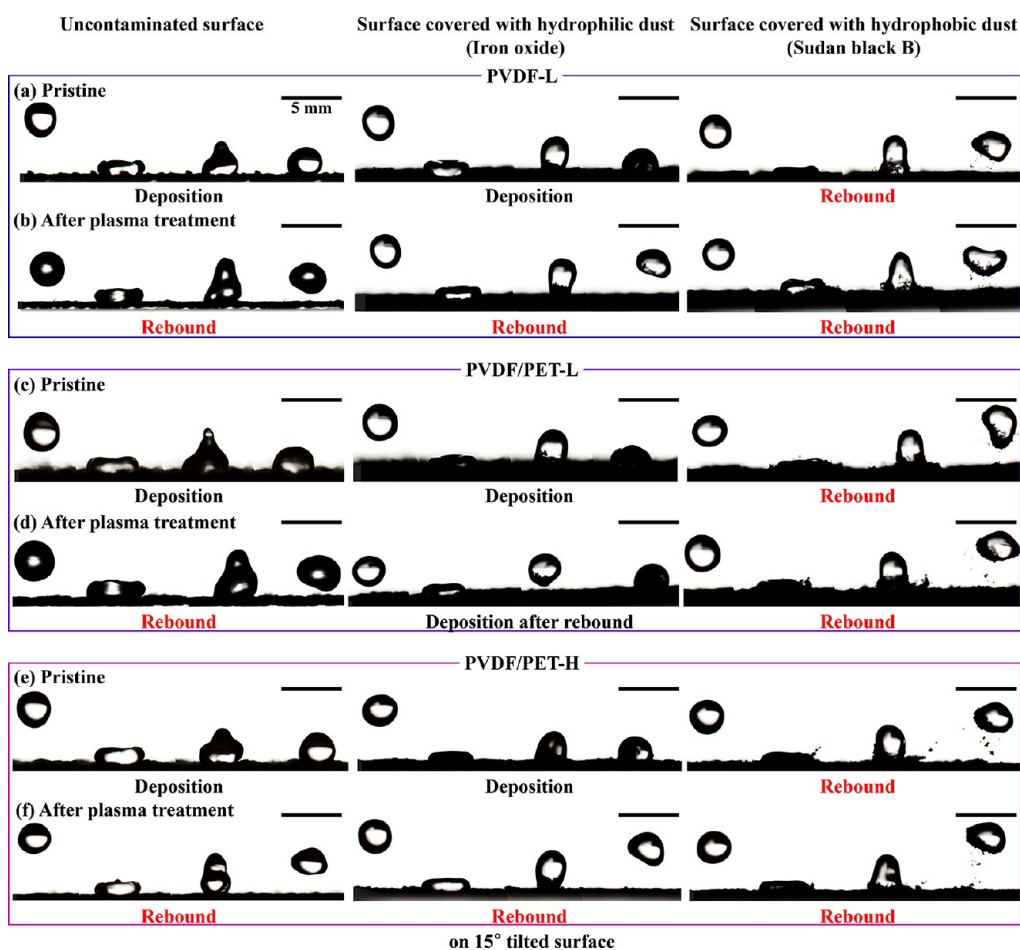
Figure 6. Effects of hydrophilic dust (iron oxide) and hydrophobic dust (Sudan black B) on the dynamic behaviors of droplets on the surfaces of (a,b) PVDF-L, (c,d) PVDF/PET-L, and (e,f) PVDF/PET-H, (a,c,e) before and (b,d,f) after plasma treatment, when a water droplet (12.5 μL volume) fell on a 15° inclined surface from a height of 1 cm. The scale bar in each image represents 5 mm. The surface inclination angle was 15°.

droplet. The above observations can be accounted for by considering that when a hydrophilic dust particle comes into contact with a water droplet, it penetrates the droplet and becomes suspended, whereas in the case of hydrophobic dust, the dust particles adsorb onto the droplet surface.[37] As a result, the hydrophilic-dust-covered surface behaves identically to the uncontaminated surface. In contrast, when a droplet falls onto a hydrophobic-dust-covered surface, the area of direct contact and the adhesion between the droplets and the fabric are reduced due to the presence of the surface-adsorbed dust. Additionally, it is believed that the hydrophobic dust increases the surface roughness,[38] thereby increasing the capillary pressure that repels droplets, creating an advantageous environment for droplet rebound.

To determine the self-cleaning properties of the fabrics, a surface inclination angle of 15° was employed, and droplets with a volume of 12.5 μL were dropped one by one onto the same position from a height of 1 cm. The dust on the surface was removed during this process, the entire process was photographed and digitalized, and the histograms obtained from the black and white images of the surface were extracted and analyzed. Thus, Figure 7 shows the results obtained for hydrophilic dust removal on plasma-treated PVDF/PET-H. More specifically, as shown in Figure 7a, prior to covering the surface with the dust, the most frequent pixels had a brightness intensity of ~161, whereas, in contrast, the most frequent pixels

for the dust-covered surface had a brightness intensity of ~17. As a greater number of water droplets fell onto the dust-coated surface, the peak area decreased around the brightness value of 17 but increased around 161, indicating that the dust was gradually removed. In addition, Figure 7b shows the cumulative distribution of the pixel brightness values of the uncontaminated surface integrated from 255. A pixel brightness intensity value of 109, where the cumulative distribution ratio reached 99.5%, was used as a threshold value to obtain the degree of dust coverage (Figure 7c). The self-cleaning efficiency (%) was then calculated as outlined in eq 4

$$\text{self-cleaning efficiency (\%)} = \left(1 - \frac{A_N}{A_0}\right) \times 100\% \tag{4}$$

where A_N is the area fraction of dust to the total area of the surface after dropping N water droplets (N = 1, 2, ..., 9, 10), and A_0 is the area fraction of dust to the total area before water droplet addition. The self-cleaning efficiency was calculated to be 7.8% for the first droplet and 29.6% for the tenth droplet.

Based on the above results, the self-cleaning efficiencies of the fabrics before and after plasma treatment are presented in Figure 8a,b, respectively. As shown, PVDF-L exhibited the highest removal rate for both iron oxide and Sudan black B due to the fact that this fabric possessed the lowest surface energy and because the PVDF filament yarns have a higher fiber density than PET filament yarns. As a result, dust adhesion or
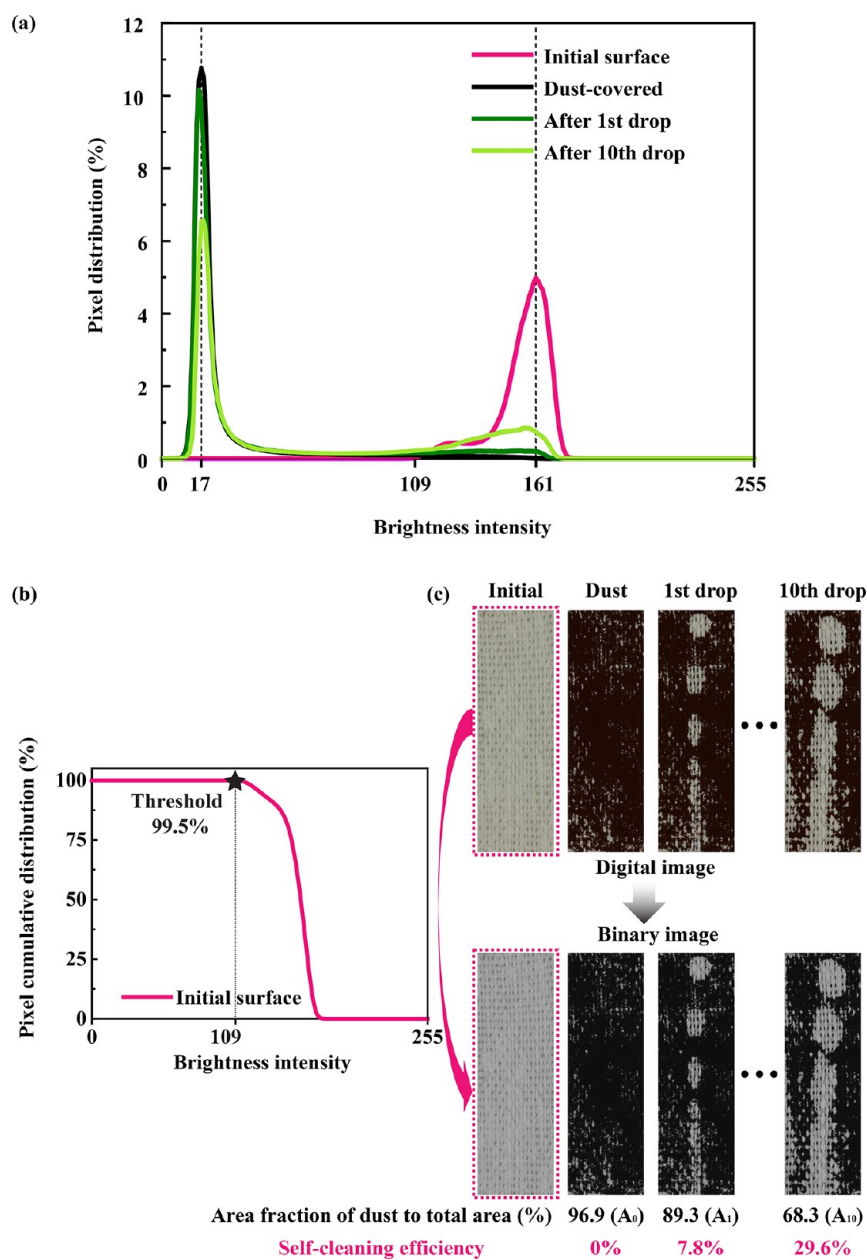
Figure 7. Example of calculating the self-cleaning efficiency of a textile. (a) Changes in the pixel distribution and (c) area fraction of dust, following hydrophilic dust (iron oxide) removal when a 12.5 μL water droplet fell from a height of 1 cm on a 15° inclined surface based on (b) the threshold value derived from the cumulative pixel distribution of PVDF/PET-H after treatment with O_2 plasma for 12 min and CF_4 plasma for 4 min.

penetration becomes more difficult, thereby facilitating dust removal. In the case of PVDF/PET-H, this fabric had the highest weave density and the highest inherent surface roughness, which resulted in a large surface area for hydrophobic dust adhesion and penetration, thereby creating unfavorable conditions for dust removal.

It was also found that plasma treatment increased the self-cleaning efficiencies of all fabrics by decreasing the adhesion between the water droplets and the surfaces, allowing the water droplets to be detached more easily (Figure 8c−f). Additionally, because the contact area between the dust and the surface was reduced due to the nanoscale roughness introduced by surface treatment, the van der Waals forces decreased, ultimately facilitating dust detachment from the surface.[37]

With the exception of the PVDF/PET-L specimen, the fabrics showed higher self-cleaning efficiencies toward the hydrophilic

particles compared to the hydrophobic particles after plasma treatment. This can be accounted for by considering that in comparison to a surface covered by hydrophobic dust, a surface covered by hydrophilic dust has a larger droplet contact area and shows superior dust removal after spreading of the fallen water droplets. In addition, the hydrophilic dust has higher specific gravity than the hydrophobic dust, which means that the weight of the droplet absorbing the hydrophilic dust will increase to a greater extent, even if the droplets carry the same amount of dust. Owing to this increased weight, when a water droplet rebounds and impinges again on the surface, it can spread further. As a result, the hydrophilic dust, in contrast to the hydrophobic dust, does not promote droplet rebound. Indeed, in the case of a hydrophilic-dust-covered surface, the droplet energy decreases to a greater extent as the displacement distance increases, leading to a shorter rebound interval. Consequently,
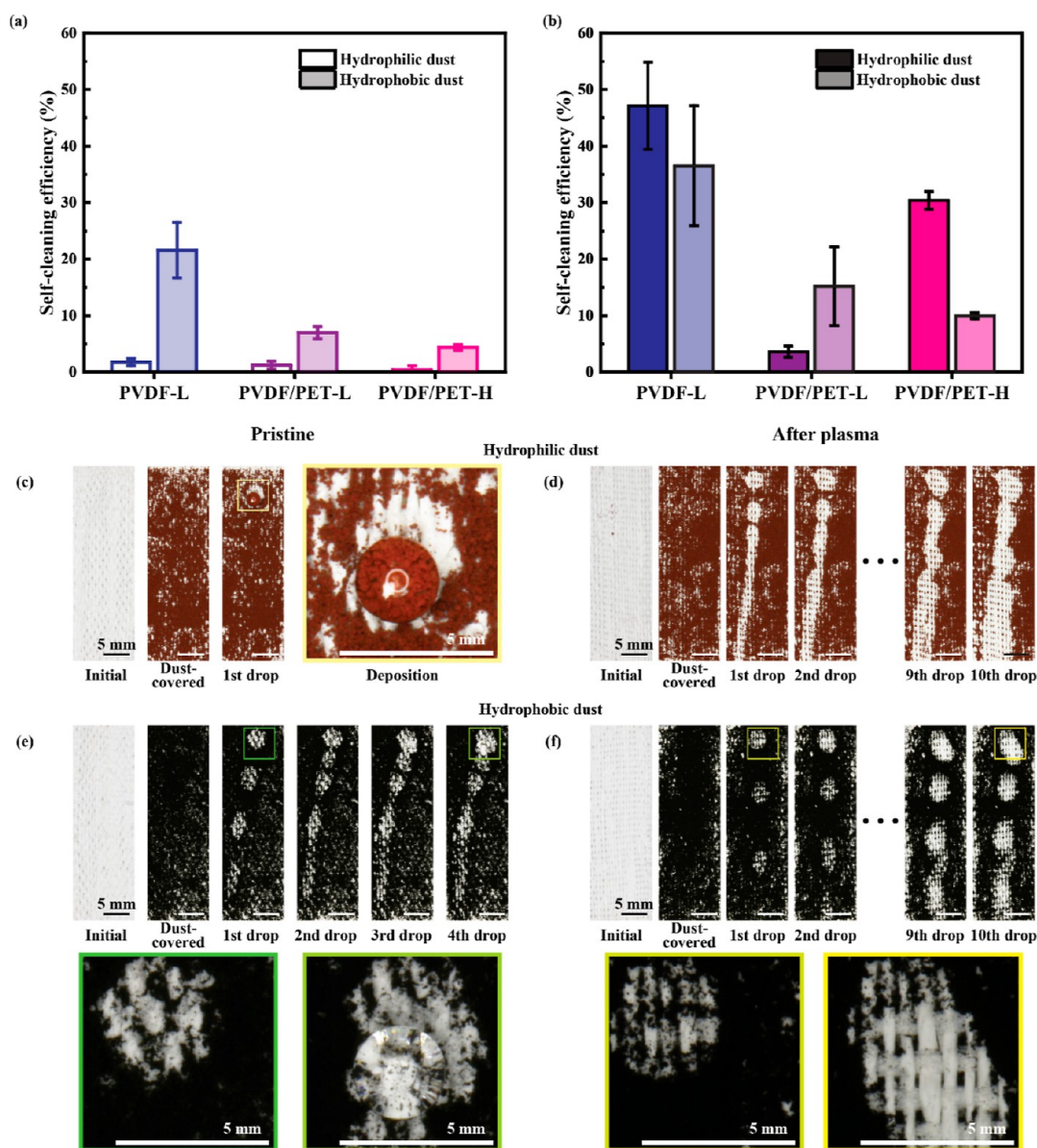
Figure 8. Self-cleaning properties of the PVDF specimens (a,c,e) before and (b,d,f) after plasma treatment. (a,b) Self-cleaning efficiencies after the last droplet (volume = 12.5 μL) fell from a height of 1 cm onto a 15° inclined surface. Cleaning processes for the surfaces contaminated with (c, d) hydrophilic (iron oxide) and (e,f) hydrophobic (Sudan black B) dust upon dropping water droplets until they accumulated on the PVDF/PET-H surface. The scale bar in each image represents 5 mm.
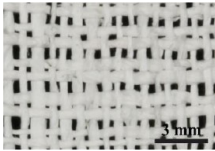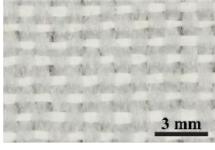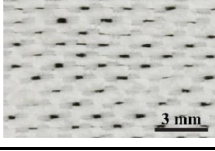
the droplets roll along the surface, increasing their contact area with the dust-covered surface. Furthermore, the minimum particle size for the hydrophilic dust is larger than the spacing between the nanostructures present on the plasma-treated surface, whereas the hydrophobic dust has a smaller particle size, allowing it to penetrate the surface nanostructures. Thus, the hydrophilic dust is believed to be adsorbed on the surface, resulting in more favorable conditions for its removal.[38,39]

3. CONCLUSIONS

This study aimed to develop superhydrophobic PVDF fabrics and examine the effects of the fabric structure on the droplet dynamics of water droplets and self-cleaning properties. Unlike the PVDF film, all fabrics became superhydrophobic after treatment with O_2 plasma for 12 min and CF_4 plasma for 4 min, and the shedding angles for the various fabrics followed the same order as that before treatment. The PVDF fabric composed of

electrospun PVDF filament yarns exhibited the smallest shedding angle. In addition, the high-density PVDF/PET fabric possessed a higher surface roughness and a smaller shedding angle than the low-density PVDF/PET fabric. Furthermore, after plasma treatment, favorable conditions were created for droplet rebound and self-cleaning in all fabrics, wherein the PVDF fabric exhibited the highest possibility of droplet rebound and the highest self-cleaning efficiency. Moreover, in all fabrics, a higher degree of droplet rebound was related to a higher surface inclination angle, a larger droplet volume, and a lower drop fall height. For the PVDF fabric and high-density PVDF/PET fabric, the self-cleaning efficiencies for hydrophobic dust removal were higher before the plasma treatment, but the hydrophilic dust removal efficiencies were better after the plasma treatment. It was confirmed that when the fabric surfaces are superhydrophobic enough to exhibit complete rebound of water drops, hydrophilic particles have low adhesion to the

Table 3. Sample Codes and Characteristics of the Fabric Specimens

Sample code	Surface image	Weave type	Weave density [inch^{-1}]	Thickness [mm]
PVDF-L		100% PVDF plain weave	24×24	1.234
PVDF/PET-L		PVDF/PET plain weave	24×24	1.240
PVDF/PET-H		PVDF/PET 2/2 weft rib weave	38×42	1.079

surface and are included inside the droplets, resulting in better removal. The findings of this study are therefore expected to contribute to the development of effective methods of weaving, treating, and employing superhydrophobic PVDF fabrics. The successful superhydrophobic modification implies that PVDF fabrics can easily be endowed with water repellency and self-cleaning properties, resulting in energy harvesting performance stabilization, which is expected to be beneficial in the development of materials for smart textiles.

4. MATERIALS AND METHODS

4.1. Materials. Three different fabrics, namely, PVDF-L, PVDF/PET-L, and PVDF/PET-H, were employed for the purpose of this study and were provided by Yeungnam University (South Korea). Photographic surface images and select characteristics of these fabrics are presented in Table 3. The fabrics were composed of PVDF filament yarns and commercial PET filament yarns with two different specifications, that is, 300D/96F×3fly and 255D/84F. PVDF-L was woven with PVDF warp and weft yarns at a density of 24 yarns per inch, while PVDF/PET-L was woven with PVDF weft and PET warp yarns using 300D/96F×3fly PET at a density of 24 yarns per inch. In addition, PVDF/PET-H was woven with PVDF weft and PET warp yarns using two yarns of 255D PET filament yarns interlaced with each weft yarn at a density of 38×42 yarns per inch. It should be noted here that PVDF/PET-H is thinner and has a higher density than PVDF-L and PVDF/PET-L.

To remove the impurities present on the fabrics, a solution containing sodium dodecylbenzene (5 g L^{-1}) sulfonate and anhydrous sodium carbonate (5 g L^{-1}) was prepared in distilled water and diluted (dilution ratio 1:30). All fabrics were immersed in the resulting diluted solution for 45 min prior to drying at room temperature. Each fabric was analyzed in the weft direction parallel to the PVDF filament yarns. To determine the contact angle with a flat surface and to analyze the effect of plasma treatment on surface properties, a commercial 100%

PVDF film (thickness: 0.08 mm; Fils Co., Ltd., South Korea) was used as the reference (Figure S5).

4.2. Plasma Treatment. The fabrics were subject to O$_2$ plasma treatment for 12 min followed by CF$_4$ plasma treatment for 4 min using a Plasmalab 80Plus system (Oxford Instrument PLC., UK). When the pressure in the plasma chamber reached 40 mTorr, etching gas was injected at a flow rate of 20 sccm, and a power of 180 W was applied. The purpose of the plasma treatment was to introduce nanoscale roughness onto the surface and to increase its hydrophobicity.

4.3. Characterization. *4.3.1. Surface Properties.* FE-SEM (SIGMA, Carl Zeiss, Germany) was employed to observe the surfaces of the fabric specimens at an acceleration voltage of 2.0 kV. To determine the thicknesses of the yarns and fibers in the fabrics, 60 points were selected from the SEM images where each yarn and fiber could be clearly distinguished, and the lengths in the direction perpendicular to the fiber axes were measured and averaged using the ImageJ software (National Institutes of Health, USA). Using a Kawabata Evaluation System (KES-FB4-A surface tester, Kato Tech Co., Ltd., Japan), the inherent surface roughness of each fabric was measured three times to obtain an average and surface mean deviation (SMD), an indicator of the geometrical roughness. To determine the percentage of area occupied by direct open pores in the fabric, the specimen surface (40 mm × 27 mm) was photographed using a digital single-lens reflex DSLR (EOS 70D, Canon) camera at three different positions, and the values were averaged (Figure S1). The compositions and distributions of the surface components on the fabrics were determined using EDS (XFlash FlatQUAD 5060F, Bruker, Germany) and XPS (AXISHis, Kratos, UK). Prior to carrying out the FE-SEM and EDS analyses, all specimens were coated with platinum at 30 mA for 100 s using a sputter coater (EM ACE200, Leica, Austria).

4.3.2. Superhydrophobicity. The static contact angle and the shedding angle between each fabric surface and a water droplet (72 dyn cm^{-1}, 20 °C distilled water) were measured using a contact angle meter to determine the surface wettability (Theta

Lite Optical Tensiometer, KSV Instruments, Finland). For the static contact angle, the angle formed after a droplet (volume 3.5 ± 0.2 μL) contacted with the surface was measured after 3 s. The shedding angle was determined as the minimum angle at which a droplet began rolling more than 2 cm on the surface when 12.5 ± 0.2 μL of distilled water was dropped vertically from a height of 1 cm onto the specimen surface.[19] The reported angles were averaged from three duplicates of five different locations on each specimen. When the static contact angle was ≥150°, and the shedding angle was ≤10°, the surface was considered to be superhydrophobic.[2]

4.3.3. Drop Dynamic Behaviors of the Water Droplets. The water droplet behaviors were determined by capturing photographic images at a rate of 3000 frames per second using a high-speed digital camera (NX3, IDT Vision, USA) to determine the water repellency. The dynamic behaviors of the water droplets on the specimen surfaces were analyzed under 45 different conditions, as listed in Table 4. The variables examined herein

Table 4. Experimental Conditions for Analyzing the Dynamic Behavior of a Droplet on the Surface

drop fall height [cm]	drop volume [μL]	surface inclination angle [°]
1.0, 7.5, 15.0	3.5, 12.5, 22.8	0, 15, 30, 45, 60

included the drop fall height, the droplet volume, and the surface inclination angle. The dynamic behaviors of the droplets were classified into four categories based on the images obtained,

namely deposition, roll, partial rebound, and complete rebound. When the droplets moved no more than 2 cm from the point of origin and remained on the surface, the behavior was classified as deposition. However, when the droplets moved in contact with the surface while maintaining a spherical or elliptical shape, the behavior was classified as a roll. In addition, the behavior was classified as a rebound when the droplets bounced off the surface at least once and moved away from the surface. Furthermore, when some of the droplets remained attached at the point of dropping, the behavior was classified as a partial rebound, but when the droplets were completely detached, the behavior was classified as a complete rebound. As previously reported, a greater probability of complete rebound was associated with an increased water repellency.[34,35] Examples of each behavior pattern are depicted in Figure 9.

4.3.4. Self-Cleaning. The self-cleaning properties of the various fabrics were quantified using iron(III) oxide (Fe_2O_3) (Daejung Chemicals & Metals Co., Ltd., South Korea) and Sudan black B (fat-soluble diazo dye, ab146284) as hydrophilic and hydrophobic dust, respectively. These particles were used to facilitate digital image processing because of their dark color, which produces a distinct contrast to the white fabric surface. The particle size was determined using a laser diffraction particle size analyzer (Mastersizer 3000, Malvern, England), and the surface morphology and composition were determined using FE-SEM and EDS, respectively.

The particles were sieved onto the fabric surface from a vertical height of 20 mm to give an area of 15 mm in the warp
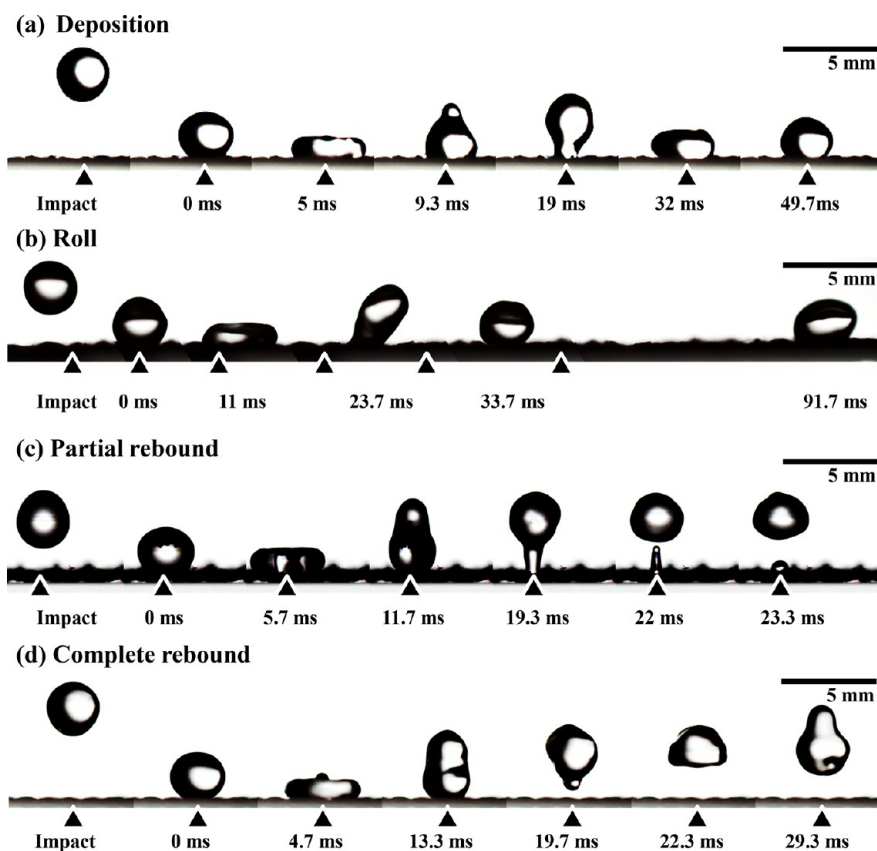

Figure 9. Categorization of the dynamic droplet behaviors on a surface. Representative examples of (a) deposition on the pristine PVDF-L (drop fall height = 1 cm, droplet volume = 12.5 μL on the horizontal plane), (b) roll on the pristine PVDF/PET-H (1 cm, 12.5 μL, 30°), (c) partial rebound on PVDF-L after plasma treatment (1 cm, 12.5 μL, 0°), and (d) complete rebound on PVDF/PET-H after plasma treatment (1 cm, 12.5 μL, 0°). *Plasma treatment conditions: O_2 plasma for 12 min and CF_4 plasma for 4 min. The initial droplet impact points in each image are indicated by triangles.

direction and 40 mm in the weft direction. The minimum weight required to completely cover the fabric surface was 0.121 ± 0.001 mg/mm^2 for iron oxide and 0.028 ± 0.001 mg/mm^2 for Sudan black B. Subsequently, on the dust-covered surface tilted at a 15° angle, droplets (12.5 μL volume) were applied from a height of 1 cm perpendicular to the surface. Droplets were applied one at a time at the same position for up to 10 times.[39] When the droplets remained attached to the surface, no additional droplets were applied.

After the application of the water droplets, the specimen surface was placed on a white background under direct illumination in a dark room with all external light sources blocked, and the specimen was photographed at a vertical distance of 33.5 cm using a DSLR camera (EOS 70D, Canon). Adobe Photoshop CS4 was used to cut a series of images to an actual area of 12 mm × 38 mm at the same position, and the image noise was filtered using the median filter (radius: 1 pixel). Subsequently, the RGB images were converted to black-and-white images using ImageJ software. The black-and-white images were composed of pixels with brightness intensity values ranging from 0 (black) to 255 (white). The histogram of the original fabric surface image prior to dust covering was extracted, and the pixel brightness intensity at a cumulative distribution of 99.5% was set as the threshold to differentiate the fabric and the dust. The image obtained during the self-cleaning test was binarized using the threshold, and the area fraction of dust was calculated by converting the ratio of the number of dust pixels to the total number of pixels in the image to a percentage (Figure S9).

ASSOCIATED CONTENT

Supporting Information

The Supporting Information is available free of charge at https://pubs.acs.org/doi/10.1021/acsomega.2c01999.

Representative examples of surface void fractions of all fabrics composed of PVDF filament yarns; effect of the plasma treatment condition on superhydrophobicity of fabrics; SEM images of surface nanoscale roughness after treatment with O$_2$ plasma for 12 min; XPS profiles and corresponding atomic concentrations of PVDF film and PVDF/PET-H according to the plasma treatment; surface wettability of PVDF-L, PVDF/PET-L, and PVDF/PET-H according to the plasma treatment; surface structure, chemical composition, and wettability of PVDF film; evaluation of the suitability of the fabric as a clothing material; air permeability of pristine PVDF-L, PVDF/PET-L, and PVDF/PET-H; tensile strength, elongation at break, flexural stiffness, CIELAB coordinates and K/S values, air permeability, and water vapor transmission rate of the PVDF/PET-H before and after plasma treatment; evaluation of the mechanical stability of superhydrophobicity; contact angles and shedding angles of PVDF/PET-H before and after laundering, tape test, and abrasions with nylon knit; and example of analyzing the area fraction of dust to the total area to evaluate the self-cleaning properties of the fabric (PDF)

AUTHOR INFORMATION

Corresponding Author

Chung Hee Park − *Department of Textiles, Merchandising and Fashion Design and Research Institute of Human Ecology, Seoul National University, Seoul 08826, Republic of Korea;* orcid.org/0000-0002-4474-5181; Email: junghee@snu.ac.kr

Authors

Hyae Rim Hong − *Department of Textiles, Merchandising and Fashion Design and Research Institute of Human Ecology, Seoul National University, Seoul 08826, Republic of Korea;* orcid.org/0000-0001-5819-4512

Joon Seok Lee − *Department of Fiber System Engineering, Yeungnam University, Gyeongsangbuk 38541, Republic of Korea*

Complete contact information is available at:
https://pubs.acs.org/10.1021/acsomega.2c01999

Notes

The authors declare no competing financial interest.

ACKNOWLEDGMENTS

ABBREVIATIONS

EDS, energy dispersive spectrometry; XPS, X-ray photoelectron spectroscopy; FE-SEM, field-emission scanning electron microscopy; SMD, surface mean deviation (i.e., geometrical roughness); PET, polyester; PVDF, polyvinylidene fluoride; TENG, triboelectric nanogenerator

REFERENCES

(1) Liu, H.; Wang, Y.; Huang, J.; Chen, Z.; Chen, G.; Lai, Y. Bioinspired Surfaces with Superamphiphobic Properties: Concepts, Synthesis, and Applications. *Adv. Funct. Mater.* **2018**, *28*, 1707415.

(2) Li, S.; Huang, J.; Chen, Z.; Chen, G.; Lai, Y. A review on special wettability textiles: theoretical models, fabrication technologies and multifunctional applications. *J. Mater. Chem. A* **2017**, *5*, 31−55.

(3) Quan, Y.-Y.; Chen, Z.; Lai, Y.; Huang, Z.-S.; Li, H. Recent advances in fabricating durable superhydrophobic surfaces: a review in the aspects of structures and materials. *Mater. Chem. Front.* **2021**, *5*, 1655−1682.

(4) Koch, K.; Bhushan, B.; Barthlott, W. Multifunctional Surface Structures of Plants: An Inspiration for Biomimetics. *Prog. Mater. Sci.* **2009**, *54*, 137−178.

(5) Wu, S.; Du, Y.; Alsaid, Y.; Wu, D.; Hua, M.; Yan, Y.; Yao, B.; Ma, Y.; Zhu, X.; He, X. Superhydrophobic Photothermal Icephobic Surfaces Based on Candle Soot. *Proc. Natl. Acad. Sci. U.S.A.* **2020**, *117*, 11240−11246.

(6) Mokhtari, S.; Karimzadeh, F.; Abbasi, M.; Raeissi, K. Development of Super-Hydrophobic Surface on Al 6061 by Anodizing and the Evaluation of its Corrosion Behavior. *Surf. Coat. Technol.* **2017**, *324*, 99−105.

(7) Barthwal, S.; Lim, S.-H. Rapid Fabrication of a Dual-Scale Micro-Nanostructured Superhydrophobic Aluminum Surface with Delayed Condensation and Ice Formation Properties. *Soft Matter* **2019**, *15*, 7945−7955.

(8) Hu, S.; Shi, Z.; Zheng, R.; Ye, W.; Gao, X.; Zhao, W.; Yang, G. Superhydrophobic Liquid-Solid Contact Triboelectric Nanogenerator as a Droplet Sensor for Biomedical Applications. *ACS Appl. Mater. Interfaces* **2020**, *12*, 40021−40030.

(9) Cho, H.; Chung, J.; Shin, G.; Sim, J.-Y.; Kim, D. S.; Lee, S.; Hwang, W. Toward sustainable output generation of liquid-solid contact triboelectric nanogenerators: The role of hierarchical structures. *Nano Energy* **2019**, *56*, 56−64.

(10) Nguyen, V.; Yang, R. Effect of Humidity and Pressure on the Triboelectric Nanogenerator. *Nano Energy* **2013**, *2*, 604−608.

(11) Peng, F.; Liu, D.; Zhao, W.; Zheng, G.; Ji, Y.; Dai, K.; Mi, L.; Zhang, D.; Liu, C.; Shen, C. Facile Fabrication of Triboelectric Nanogenerator Based on Low-Cost Thermoplastic Polymeric Fabrics for large-Area Energy Harvesting and Self-Powered Sensing. *Nano Energy* **2019**, *65*, 104068.

(12) Zhu, M.; Shi, Q.; He, T.; Yi, Z.; Ma, Y.; Yang, B.; Chen, T.; Lee, C. Self-Powered and Self-Functional Cotton Sock Using Piezoelectric and Triboelectric Hybrid Mechanism for Healthcare and Sports Monitoring. *ACS Nano* **2019**, *13*, 1940−1952.

(13) Lee, Y.; Cha, S. H.; Kim, Y.-W.; Choi, D.; Sun, J.-Y. Transparent and Attachable Ionic Communicators Based on Self-Cleanable Triboelectric Nanogenerators. *Nat. Commun.* **2018**, *9*, 1804.

(14) Chen, A.; Zhang, C.; Zhu, G.; Wang, Z. L. Polymer Materials for High-Performance Triboelectric Nanogenerators. *Adv. Sci.* **2020**, *7*, 2000186.

(15) You, M.-H.; Wang, X.-X.; Yan, X.; Zhang, J.; Song, W.-Z.; Yu, M.; Fan, Z.-Y.; Ramakrishna, S.; Long, Y.-Z. A self-powered flexible hybrid piezoelectric-pyroelectric nanogenerator based on non-woven nanofiber membranes. *J. Mater. Chem. A* **2018**, *6*, 3500−3509.

(16) Sang, M.; Wang, S.; Liu, S.; Liu, M.; Bai, L.; Jiang, W.; Xuan, S.; Gong, X. A Hydrophobic, Self-Powered, Electromagnetic Shielding PVDF-Based Wearable Device for Human Body Monitoring And Protection. *ACS Appl. Mater. Interfaces* **2019**, *11*, 47340−47349.

(17) Song, J.; Yang, B.; Zeng, W.; Peng, Z.; Lin, S.; Li, J.; Tao, X. Highly Flexible, Large-Area, and Facile Textile-Based Hybrid Nanogenerator with Cascaded Piezoelectric and Triboelectric Units for Mechanical Energy Harvesting. *Adv. Mater. Technol.* **2018**, *3*, 1800016.

(18) Lee, D. W.; Jeong, D. G.; Kim, J. H.; Kim, H. S.; Murillo, G.; Lee, G.-H.; Song, H.-C.; Jung, J. H. Polarization-Controlled PVDF-Based Hybrid Nanogenerator for an Effective Vibrational Energy Harvesting from Human Foot. *Nano Energy* **2020**, *76*, 105066.

(19) Zimmermann, J.; Seeger, S.; Reifler, F. A. Water Shedding Angle: A New Technique to Evaluate the Water-Repellent Properties of Superhydrophobic Surfaces. *Text. Res. J.* **2009**, *79*, 1565−1570.

(20) Zhang, X.-S.; Han, M.-D.; Wang, R.-X.; Meng, B.; Zhu, F.-Y.; Sun, X.-M.; Hu, W.; Wang, W.; Li, Z.-H.; Zhang, H.-X. High-performance triboelectric nanogenerator with enhanced energy density based on single-step fluorocarbon plasma treatment. *Nano Energy* **2014**, *4*, 123−131.

(21) Lee, C.; Yang, S.; Choi, D.; Kim, W.; Kim, J.; Hong, J. Chemically surface-engineered polydimethylsiloxane layer via plasma treatment for advancing textile-based triboelectric nanogenerators. *Nano Energy* **2019**, *57*, 353−362.

(22) Prada, T.; Harnchana, V.; Lakhonchai, A.; Chingsungnoen, A.; Poolcharuansin, P.; Chanlek, N.; Klamchuen, A.; Thongbai, P.; Amornkitbamrung, V. Enhancement of output power density in a modified polytetrafluoroethylene surface using a sequential O2/Ar plasma etching for triboelectric nanogenerator applications. *Nano Res.* **2022**, *15*, 272−279.

(23) Balu, B.; Breedveld, V.; Hess, D. W. Fabrication of "roll-off" and "sticky" superhydrophobic cellulose surfaces via plasma processing. *Langmuir* **2008**, *24*, 4785−4790.

(24) Balu, B.; Kim, J. S.; Breedveld, V.; Hess, D. W. Tunability of the adhesion of water drops on a superhydrophobic paper surface via selective plasma etching. *J. Adhes. Sci. Technol.* **2009**, *23*, 361−380.

(25) Hopkins, J.; Badyal, J. CF$_4$ plasma treatment of asymmetric polysulfone membranes. *Langmuir* **1996**, *12*, 3666−3670.

(26) Sigurdsson, S.; Shishoo, R. Surface properties of polymers treated with tetrafluoromethane plasma. *J. Appl. Polym. Sci.* **1997**, *66*, 1591−1601.

(27) Tressaud, A.; Durand, E.; Labrugère, C. Surface modification of several carbon-based materials: comparison between CF$_4$ rf plasma and direct F$_2$-gas fluorination routes. *J. Fluorine Chem.* **2004**, *125*, 1639−1648.

(28) Wenzel, R. N. Resistance of Solid Surfaces to Wetting By Water. *Ind. Eng. Chem. Res.* **1936**, *28*, 988−994.

(29) Cassie, A.; Baxter, S. Wettability of Porous Surfaces. *Trans. Faraday Soc.* **1944**, *40*, 546−551.

(30) Jiang, J.; Zhu, L.; Zhu, L.; Zhu, B.; Xu, Y. Surface Characteristics of a Self-Polymerized Dopamine Coating Deposited on Hydrophobic Polymer Films. *Langmuir* **2011**, *27*, 14180−14187.

(31) Huang, X. J.; Kim, D. H.; Im, M.; Lee, J. H.; Yoon, J. B.; Choi, Y. K. "Lock-and-Key" Geometry Effect of Patterned Surfaces: Wettability and Switching of Adhesive Force. *Small* **2009**, *5*, 90−94.

(32) Oh, J. H.; Park, C. H. The Effect of Fiber Type and Yarn Diameter on Superhydrophobicity, Self-Cleaning Property, and Water Spray Resistance. *Polymers* **2021**, *13*, 817.

(33) Kim, S.; Oh, J. H.; Park, C. H. Development of Energy-Efficient Superhydrophobic Polypropylene Fabric by Oxygen Plasma Etching and Thermal Aging. *Polymers* **2020**, *12*, 2756.

(34) Chen, L.; Xiao, Z.; Chan, P. C.; Lee, Y.-K.; Li, Z. A Comparative Study of Droplet Impact Dynamics on a Dual-Scaled Super-hydrophobic Surface and Lotus Leaf. *Appl. Surf. Sci.* **2011**, *257*, 8857−8863.

(35) Deng, T.; Varanasi, K. K.; Hsu, M.; Bhate, N.; Keimel, C.; Stein, J.; Blohm, M. Nonwetting of Impinging Droplets on Textured Surfaces. *Appl. Phys. Lett.* **2009**, *94*, 133109.

(36) LeClear, S.; LeClear, J.; Abhijeet; Park, K. C.; Choi, W. Drop impact on inclined superhydrophobic surfaces. *J. Colloid Interface Sci.* **2016**, *461*, 114−121.

(37) Quan, Y. Y.; Zhang, L. Z.; Qi, R. H.; Cai, R. R. Self-cleaning of surfaces: the role of surface wettability and dust types. *Sci. Rep.* **2016**, *6*, 38239.

(38) Geyer, F.; D'Acunzi, M.; Sharifi-Aghili, A.; Saal, A.; Gao, N.; Kaltbeitzel, A.; Sloot, T.-F.; Berger, R.; Butt, H.-J.; Vollmer, D. When and how Self-Cleaning of Superhydrophobic Surfaces Works. *Sci. Adv.* **2020**, *6*, No. eaaw9727.

(39) Milles, S.; Soldera, M.; Kuntze, K.; Lasagni, A. F. Characterization of Self-Cleaning Properties on Superhydrophobic Aluminum Surfaces Fabricated by Direct Laser Writing and Direct Laser Interference Patterning. *Appl. Surf. Sci.* **2020**, *525*, 146518.